Article

Atoms Dressed by Virtual and Real Photons

Maria Allegrini [1,2] and **Ennio Arimondo** [1,3,*]

1   Dipartimento di Fisica "E. Fermi", Università di Pisa, Largo B. Pontecorvo 3, I-56127 Pisa, Italy; maria.allegrini@unipi.it
2   Istituto Nanoscienze, Consiglio Nazionale delle Ricerche (NANO-CNR), I-56127 Pisa, Italy
3   Istituto Nazionale di Ottica (INO-CNR), Sede Secondaria di Pisa, via G. Moruzzi 1, I-56124 Pisa, Italy
*   Correspondence: ennio.arimondo@unipi.it

Abstract: Specific properties of quantum field theory are described by considering the combination of the system under investigation and the cloud of virtual or real particles associated with the field. Such a structure is called a "dressed system", in contrast with the bare one in the absence of the interaction with the field. The description of the properties of such clouds in various physical situations is, today, an active research area. Here, we present the main features associated with virtual and real dressings, focusing on photon dressing. In analogy to virtual photon clouds dressing electrons in vacuum, virtual phonon clouds appear in solid-state physics. The interaction between real photons and the schematized two-level structure of an atom paves the way to flexible quantum control. Here, a unifying Floquet engineering approach is applied to describe single- and multiple-dressed atom configurations. Connections with the past and present atomic physics experiments are presented.

Keywords: dressed atom; multiple dressing; virtual and real photons

1. Introduction

Light is a key element of human life, regulating day-to-night evolution, the succession of the seasons, and even providing relics of the early evolution of the universe. Its description has attracted significant attention from physicists, initially based on electromagnetic wave theory, and later on photon quantum theory. Today, photons are at the core of advanced quantum technologies. The new targets include the modification and control of the quantum properties of the system under investigation. Quantum variables, energies, and observables can be manipulated by single, bichromatic, or multiple photon excitations. The long-term dynamics of a quantum system are altered by time-periodic driving. These dynamics are well captured by time-independent effective Hamiltonians that account for the essential characteristics of the modulated system. This approach, known as Floquet engineering, represents a versatile scenario for producing unusual quantum properties that are difficult to engineer directly. Within this quantum control scenario, the so-called "dressing" of a quantum system by resonant or off-resonant photons is an important tool, as it modifies the energy and electromagnetic response of any generic quantum system through photon dressing.

Franco Persico and collaborators have extensively used the dressed model to describe the interaction between an atomic system and photons, as reviewed in their 1995 book [1]. Two definitions of dressed states are present in the literature, associated with the interaction with either virtual or real photons. In Section 2, we recall the main features of systems dressed by either photons or phonons. In Section 3, we elaborate on the photon dressing of atomic states. We deal with the Hamiltonian of a two-level quantum system, excited by a strong resonant or non-resonant field, with energy separation regulated by an applied magnetic field. The spin temporal evolution is derived based on the Floquet engineering approach, reviewed in Refs. [2–4]. The most important features of dressed atom systems are recalled and linked to experimental observations. Section 3 is concluded by a study of

multiple dressings, i.e., driving by several modes of the applied real photons. Section 4 completes the paper with discussion of the work done and perspectives.

2. Dressed States

The concept of a dressed state in quantum field theory was introduced independently at different times in various physics contexts. As reported in the 2006 review by Persico and collaborators [5], a dressing system was first introduced by Van Hove [6] and illustrated in Feynman's book on quamtum electrodynamics (QED) [7]. The concept proposes a general criterion to describe the combined states of a quantum field and its source, where the source is consistently associated with a cloud of photons from the produced field. In a ground-state quantum system, a real wave cannot be emitted, and only virtual processes occur. As a typical example in nuclear physics, a dressed state consists of a static nucleon source with mesons emitted and reabsorbed by the nucleon. In solid-state physics, polarons, as named by Solomon Pekar [8], are associated with an electron or an exciton dressed by a cloud of virtual phonons. Such an electron, along with the accompanying deformation, moves freely across the crystal but with an increased effective mass [9,10]. Also, other charged particles such as holes, ions, and impurities in a Bose–Einstein condensate, follow the polaron model of a dressed system [11].

Given that a neutral atom can absorb and emit virtual photons, dressed atom cloud effects should be considered in quantum–electrodynamics, similar to meson and polaron cases. The photon cloud is characterized by one-photon fluctuations, whose timescale is determined by the inverse of the atomic emission frequency. For typical optical fields, within this timescale, photons propagate up to a distance smaller than 0.1 μm [12]. Considerations in Refs. [13–15] indicate that the retarded long-range interatomic van der Waals forces originate from the interaction of one atom with the photon fluctuation fields of another atom. Additionally, Casimir forces can be interpreted as long-range forces induced by vacuum fluctuations of the absorption/emission processes [16]. Physical effects related to the virtual photon cloud, such as self-energy shifts, mass, and charge renormalization, are expected when probed at these short propagation times. However, experimental features of this topic, known as zero-point field dressing [12], remain largely unexplored. The sequence of random photon absorption/emission events produced by the virtual photon dressing cannot be described by the Floquet engineering of quantum control.

The second notion of dressing, originating in the context of atomic physics and referred to as strong field dressing in Ref. [12], is associated with real photons. In this scenario, the presence of an excited state for the atom (or molecule) plus field system is crucial. In basic analysis, the bare atom is depicted as a two-level system, and a strong monochromatic (or multi-chromatic) field is supplied by an external source. This intense radiation field mixes and splits the levels of the entire system, completely overshadowing the action of vacuum fluctuations. The energy eigenstates of the entire system exhibit correlations between the bare atomic occupation states and the photon numbers, resulting in the creation of entangled states. The eigenvalue spectrum of this coupled system differs significantly from that of the states dressed by vacuum fluctuations as discussed in this Section just above.

The study of these real photon-dressed states follows two different paths. As in the 1995 book by Persico and collaborators [1], the focus could be on the optical photon regime, where the photon energy is greater than the atom-field interaction. In this regime, the rotating-wave approximation (RWA) significantly simplifies the Hamiltonian. This approach leads to the Jaynes–Cummings model of quantum optics, optical pumping, laser cooling, and other phenomena [17]. Another quite an intriguing regime, denoted as strong field dressing, takes place when the energy scale of the atom–field interaction is larger than the energy of the external photons, typically in the radiofrequency (RF) or microwave (MW) range. In this case, RWA cannot be applied, and the counter-rotating component of the electromagnetic interaction cannot be disregarded. The seminal study of Laurent Cohen-Tannoudji, Serge Haroche and collaborators [18–20] first detailed the modifications of the energy levels of a spin one-half system in the presence of a strong off-resonant RF

dressing field. It was described as frequency modulation in Ref. [21], and extended to the presence of dissipation in Ref. [22]. Studies in Refs. [23,24] highlighted the close connection of this dressing case to tunneling suppression, and Ref. [4] linked the dressing to the dynamical localization freezing in optical lattices. In Ref. [25] the dressing generalization was investigated to a periodic arbitrary waveform. This off-resonant strong dressing, which is the focus of the present work, is closely linked to quantum control.

A second RF field could also be used to probe the levels of the dressed atom. This experimental approach was initiated in Ref. [26], where a weak 'tickling' field investigates the eigenstates of an atom interacting with a strong field. This point of view can be adopted for a large set of experiments with two applied RF fields: one dressing the atom and the other inducing transitions between the dressed eigenstates, as explored in Ref. [27] for the dressing of a Bose–Einstein condensate. A main advantage highlighted in Ref. [28] is that the dressing RF field is treated exactly, rather than using perturbation analyses.

Entangled dressed states composed of particles and photons can be manipulated or probed by acting on one of the two components. This one-component manipulation represents an intriguing quantum control configuration. In the laser manipulation of entangled optical photon/atom states, a spatial inhomogeneity in the dressed photon component generates dipole forces on atoms [17]. In solid-state physics, an early probe example was reported in Ref. [29]. The lattice optical modes in a semiconductor were monitored by the modifications in the magnetic de Haas–van Alphen oscillations of the electron component, owing to the presence of polaron-entangled states.

Mathematical treatments of virtual and real photon cases differ significantly. The quantized description suits virtual photons, which typically play a role in small numbers or even as a single entity. The photons entire evolution is aptly described by the creation/destruction of a single photon. The classical description of the electromagnetic field associated with photons is more suitable for real photons, which are usually present in large numbers. The atom/photon interaction changes the photon number by a few units, causing a negligible modification of the electromagnetic field's amplitude. In any configuration, a pictorial representation of atomic evolution, utilizing Feynman-type diagrams to depict photon exchanges between atoms and fields, is rather helpful.

3. Results

3.1. Dressed Hamiltonian and Spin Detection

For natural or artificial atoms in the ground electronic state, in the presence of quite a weak direct current (DC) applied magnetic field, the level structure is described by a collection of degenerate two-level systems. We examine the interaction between such a spin-one-half system and static and oscillating magnetic fields. The spin-field coupling is determined by the $\gamma = g\mu_B$ constant, with g denoting the Landé factor and μ_B denoting the Bohr magneton, assuming $\hbar = 1$. The $\vec{B}_0$ static magnetic field has components B_{0j} on the $j = x, y,$ and z axes. The qubit is driven by time-dependent, periodic, and commensurate fields, oriented along the $x, y,$ and z axes. The harmonic Hamiltonian describing such spin coupling is as follows:

$$H(t) = \frac{\gamma}{2} \left[\vec{B}_0 \cdot \vec{\sigma} + \sum_{i=x,y,z} B_i \cos(\Phi_i(t)) \, \sigma_i \right], \tag{1}$$

with t denoting the time, σ_i denoting the Pauli matrices, B_i denoting the oscillating field amplitudes, and the Φ_i phases given by

$$\Phi_i(t) = p_i \omega t + \Phi_{0i}. \tag{2}$$

Here, ω is the fundamental frequency, p_i denotes integer numbers with $p_x = 1$, Φ_{0i} denotes the initial phases of the harmonic fields. One phase can be assumed equal to zero by properly choosing the initial $t = 0$ time, with its value not modifying the eigenvalues.

By taking the ω angular frequency as the frequency unit in Equation (1), we introduce dimensionless quantities as $\tau = \omega t$ time, $\vec{\omega}_0 = \gamma \vec{B}_0 / \omega$ magnetic vector, its ω_0 modulus and components ω_{0i}, and the $\Omega_i = \gamma B_i / \omega$ Rabi frequency. In these dimensionless units, the eigenenergies of the bare atom are $\pm \omega_0 / (2\omega)$. The Hamiltonian (1) does not include relaxation processes; more precisely, those processes are negligible on the timescale of the experimental investigations.

The associated $U(\tau)$ time evolution operator results in the following:

$$i\dot{U}(\tau) = \frac{1}{2} \left[\vec{\omega}_0 \cdot \vec{\sigma} + \sum_{i=x,y,z} \Omega_i \cos(\tau + \Phi_{0i}) \sigma_i \right] U(\tau), \tag{3}$$

where the dot on the top denotes the time derivative. This operator is obtained numerically, starting from the initial condition, $U(0) = 1$, and propagating until $\tau = 2\pi$. In the case of a periodic time dependence, the Floquet theorem [2–4,30–36] allows us to write the following:

$$U(\tau) = e^{-i\mathcal{K}(\tau)} e^{-i\Lambda \tau}. \tag{4}$$

The U-operator contains the $\mathcal{K}$ kick operator with $\mathcal{K}(0) = 0$ and $\mathcal{K}(\tau + 2\pi) = \mathcal{K}(\tau)$. It describes the short time-dependent evolution over a single period of the driving field. This evolution is denoted as micro-motion dynamics [2–4], and examined in the experiments in Refs. [37,38]. The long-term evolution dynamics are determined by the Λ-operator, behaving as a time-independent Hamiltonian. This evolution corresponds to the stroboscopic dynamics at times $t = 2\pi/\omega$. The Λ-matrix is not unique since the same U-operator is obtained by subtracting multiples of the ω frequency from its diagonal elements and adding the same quantity to $\mathcal{K}(\tau)$. The Floquet matrix is numerically obtained as $\Lambda = (i/2\pi) \log U(2\pi)$. Its E_+^n and E_-^n eigenvalues are periodic with the ω frequency and given by the following sequences:

$$E_+^n = (\lambda_+ + n)\omega, \quad E_-^n = (\lambda_- + n)\omega, \tag{5}$$

with the n integer. Additionally, $\lambda_+ = -\lambda_-$, with their sum remaining constant for both bare and dressed eigenenergies [31]. The λ_+ and λ_- Floquet eigenenergies are restricted to the $(-1/2, +1/2)$ interval, denoted as the first Brillouin zone associated with the eigenenergy periodicity [39]. The Λ matrix can be written as follows:

$$\Lambda = \frac{1}{2\omega} \vec{h} \cdot \vec{\sigma}. \tag{6}$$

The $\vec{h}$ vector, measured in energy units, represents an effective magnetic field, with the maximum absolute value equal to the dressing frequency. From a quantum simulation–stroboscopic point of view, the stroboscopically-dressed qubit is described by an effective Hamiltonian associated with the $\vec{h}$ field. The long-term spin time evolution is determined by the dressed Larmor frequency, Ω_L, being the modulus of the $\vec{h}$ vector, given as follows:

$$\Omega_L = |\lambda_+ - \lambda_-|\omega. \tag{7}$$

The spin response characterized by the dressed Larmor frequency of Equation (7) is described here by an effective gyromagnetic ratio, g_{eff}, defined as

$$g_{\text{eff}} = \Omega_L / \omega_0, \tag{8}$$

representing the equivalent of the effective mass introduced to describe the phonon dressing of the polaron [9]. The Λ-operator eigenstates correspond to the spin, oriented parallel or antiparallel to the $\vec{h}$ vector, along the direction defined by the $\vec{u}$ orientation unit vector, with

$$\vec{u} = \vec{h} / \Omega_L. \tag{9}$$

Plots of $\lambda_\pm$ or Ω_L versus control parameters provide the key information on the dressed spin response. The spin time evolution contains additional components produced by the kick operator centered around the multiple of the ω dressing frequency measured in the dual-dressing investigation in Refs. [37,38,40].

The detection of the spin response is an important additional issue. Over the years, theoretical descriptions have followed experimental evolutions. The early RF/MW investigations of optically pumped atoms provided the sensitivity required to explore the dressed systems. The detection was restricted to the RF/MW absorption, with an experimental enhancement factor given by the ratio between the detected optical photons and the dressing photons. The spin sample was prepared in one eigenstate of the bare atom, and the occupation of the other eigenstate was monitored by the light absorption. As required for atoms with random velocities and, therefore, random interaction times, in Refs. [30,41,42] a time-averaged probability, $\langle P \rangle$, is derived from the dressed eigenenergies and results to

$$\langle P \rangle = \frac{1}{2} \left[1 - \left(\frac{\partial \Omega_L}{\partial \omega_0} \right)^2 \right]. \tag{10}$$

Lately, monitoring the spin transverse magnetization $\langle \sigma_i(t) \rangle$, $i = x, y$, for instance, by Faraday detection, has provided a more effective detection tool, mainly with ultracold atoms [40,43–46]. In this configuration, the spin system is initially prepared in a superposition of the bare atom eigenstates; for instance, the $\langle \sigma_x(t = 0) \rangle = 1$ mean value and the $\langle \sigma_y(t) \rangle$ mean value of the dressed atom eigenstates, oscillating mainly at Ω_L, is monitored. The dressed atom time evolution is derived from the evolution operator of Equation (4).

3.2. Single x Strong Dressing

The single *x* strong dressing configuration is described by the evolution operator of Equation (3) with $\Omega_y = \Omega_z = 0$ and $\Omega_x \gg \omega_0$:

$$i\dot{U}(\tau) = \frac{1}{2}[\vec{\omega}_0 \cdot \vec{\sigma} + \Omega_x \cos(\tau)\, \sigma_x]U(\tau), \tag{11}$$

with the $\Phi_{0x} = 0$ initial condition. This configuration was introduced as the "dressed atom" in Refs. [18–20]. The spin response was examined for atoms in Refs. [27,47–52], for a Bose–Einstein condensate in Ref. [53], for a two-dimensional electron gas in Ref. [54], and for the control of a strong spin-exchange relaxation in Ref. [55]. This strong dressing was applied in Refs. [56,57] to compensate for an inhomogeneous spin distribution, and applied to an inhomogeneous dressing field in Ref. [58]. Its characteristic feature is a collapse/crossing of the dressed atom eigenvalues for a specific value of the dressing field amplitude. A regime—denoted as critical dressing based on the simultaneous dressing of two spin species to the same dressed Larmor precession frequency—was explored in Refs. [59–62].

The photon number basis is quite a practical tool for time evolution, even in the strong atomic dressing with a classical description of the electromagnetic field, as schematically shown in Figure 1a. The atomic evolution shown by the vertical black line evidences interactions with photons shown by the blue dots. Photons of a specific circular polarization, closely resonant with the atomic energy splitting, lead to real absorption-emission processes. Those of the opposite polarization and non-resonant result in virtual absorption–emission processes. For the case where $\omega_{0z} \ll \omega$ in dressing, this real-virtual separation becomes less strict. In addition, in the presence of strong driving, interferences between the individual processes depicted in Figure 1 become significant, and the photon model alone cannot provide complete information.
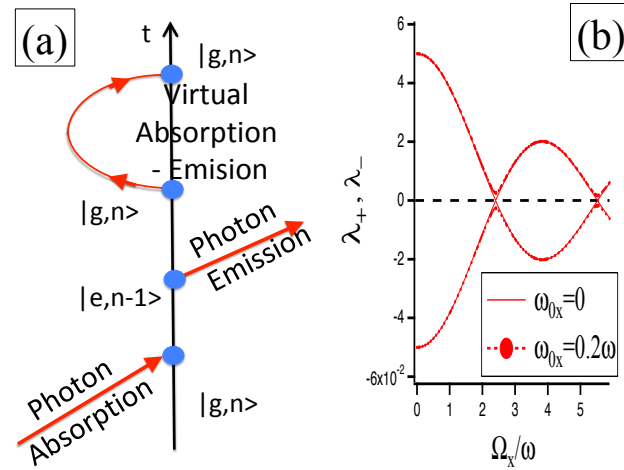
Figure 1. Strong x single dressing configuration. (**a**) The scheme of the time evolution for the atom–photon interaction within the basis of the $|g, n\rangle, |e, n\rangle$ atomic states, with g denoting ground atomic state, e the excited one, and the n photon number. For the spin-1/2 system, the σ photons of one polarization produce real absorption–emission transitions, while those of opposite polarization produce virtual transitions. (**b**) λ_+ and λ_- Floquet eigenenergies versus the Ω_x/ω. Here, $\omega_{0z} = 0.2\omega$, $\omega_{0y} = 0$. At the anticrossing points of the dashed line, the dressed Larmor frequency, Ω_L, given by the difference of the eigenenergies, is equal to ω_{0z}. See text for details.

Introducing the U_I interaction representation with respect to the strong Ω_x dressing field, the U time evolution operator is factorized as [46]

$$U(\tau) = e^{-i\varphi_x\sigma_x/2} U_I(\tau), \tag{12}$$

where

$$\varphi_x(\tau) = \frac{1}{2}\tilde{\Omega}_x \sin(\tau), \tag{13}$$

and

$$\tilde{\Omega}_x = \Omega_x/\omega. \tag{14}$$

The gauge transformation of Equation (12) represents a unitary change to a reference frame rotating around the x-axis with the $\varphi_x(\tau)$ rotation angle presenting a sinusoidal time dependence, i.e., a frequency-modulated rotation, as denoted in Ref. [63]. Applying the Floquet transformation of Equation (4) to the U_I time evolution, the gauge transformation becomes

$$U(\tau) = e^{-i\varphi_x\sigma_x/2} U_I(\tau) = e^{-i\varphi_x\sigma_x/2} e^{-i\mathcal{K}(\tau)} e^{-i\Lambda\tau}, \tag{15}$$

where the $-i\varphi_x\sigma_x/2$ exponent contributes to the micro-motion. The U_I operator is written, here and also in the following cases, as

$$i\dot{U}_I(\tau) = A^x(\tau)U_I, \tag{16}$$

with the present $A^x(\tau)$ matrix given by

$$A^x(\tau) = e^{i\varphi_x\sigma_x/2} \frac{1}{2}\vec{\omega}_0 \cdot \vec{\sigma} e^{-i\varphi_x\sigma_x/2}$$
$$= \frac{\omega_{0x}}{\omega}\sigma_x + \left(\frac{\omega_{0y}}{2\omega}\cos(\varphi_x) + \frac{\omega_{0z}}{2\omega}\sin(\varphi_x)\right)\sigma_y + \left(-\frac{\omega_{0y}}{2\omega}\cos(\varphi_x) + \frac{\omega_{0z}}{2\omega}\sin(\varphi_x)\right)\sigma_z. \tag{17}$$

In Equation (17), the following relation is used:

$$e^{i\varphi_x(\tau)} = \cos(\varphi_x(\tau)) + i\sin(\varphi_x(\tau)) = \sum_n J_n(\tilde{\Omega}_x)e^{in\tau}, \tag{18}$$

where J_n represents the n-th order Bessel function.

Applying the Floquet–Magnus expansion, as discussed in Refs. [3,34], to the $U_I(\tau)$ operator, we derive $\mathcal{K} = \mathcal{K}^1 + ...$ and $\Lambda = \Lambda^1 + ...$, where the first terms are

$$\Lambda^1 = \frac{1}{2\pi} \int_0^{2\pi} A(\tau) d\tau, \quad \mathcal{K}^1(\tau) = \int_0^{\tau} A(\tau') d\tau' - \tau \Lambda_1. \tag{19}$$

Following the effective field definition of Equation (6), its first-order $\vec{h}^1$ value results in

$$\vec{h}^1 = \begin{pmatrix} \omega_{0x} \\ J_0(\tilde{\Omega}_x)\omega_{0y} \\ J_0(\tilde{\Omega}_x)\omega_{0z} \end{pmatrix}. \tag{20}$$

In the same order, the dressed Larmor frequency results in the following:

$$\Omega_L^1 = \sqrt{\omega_{0x}^2 + \left(\omega_{0y}^2 + \omega_{0z}^2\right)\left(J_0(\tilde{\Omega}_x)\right)^2}. \tag{21}$$

The $\vec{u}$ spin orientation vector is obtained using Equation (9). High-order corrections to the single strong dressing response are reported in Refs. [64–70], in a few cases, based on semiclassical approaches.

The spin dressing produces a uniaxial modification of the magnetic response, depending on the spatial direction of the applied static magnetic field, namely the undressed response along the dressing field, the x direction, and the $J_0(\tilde{\Omega})$ scaled one in the orthogonal plane. This anisotropy of the $\vec{h}^1$ effective magnetic response was verified experimentally in Ref. [20]. Notably, a collapse of the magnetic energies associated with the y and z directions for the Ω_x/ω parameters corresponding to a zero of the J_0 function is present. For $\omega_{0x} = \omega_{0y} = 0$, we derive from Equation (8) $g_{\text{eff}} = J_0(\tilde{\Omega}_x)$, which characterizes that collapse.

The Floquet eigenenergies are plotted in Figure 1b versus the Ω_x field for different ω_{0x} values. These plots evidence an issue common to all dressed atom eigenenergies versus a control parameter: the presence of crossings and anticrossings in the eigenenergies spectra. The postions of crossings and anticrossings positions are characteristic of a specific dressing process. Spectra crossings appear for $\omega_{0x} = 0$ at the crossing/collapse values corresponding to the first and second zeroes of the J_0 function. Those crossings are modified into anticrossings by the presence of a static magnetic field parallel to the dressing field. For $\omega_{0y} = 0$, the Ω_L value is given by ω_{0x} at the anticrossing points. The dressed energies were measured in Ref. [27] by irradiating a dressed Bose–Einstein condensate with an additional weak RF tickling field resonant with the dressed state-level spacing. In Ref. [53], the dressed energies were derived from the confinement of a Bose–Einstein condensate atoms in an inhomogeneous static magnetic field.

The time-dependent spin precession of the dressed atom was examined theoretically in Ref. [20], and expanded in Ref. [61]. In Ref. [46] the spin precession is derived using the Floquet engineering approach. For an initial $\langle \sigma_x(0) \rangle = 1$ eigenstate, the spin expectation values are

$$\langle \sigma_x(t) \rangle = (1 - u_x^2)\cos(\Omega_L t) + u_x^2,$$
$$\langle \sigma_y(t) \rangle = [u_y \sin\varphi_x + u_z \cos\varphi_x]\sin(\Omega_L t) + [u_x u_y \cos\varphi_x - u_x u_z \sin\varphi_x](1 - \cos(\Omega_L t)),$$
$$\langle \sigma_z(\tau) \rangle = [u_z \sin\varphi_x - u_y \cos\varphi_x]\sin(\Omega_L t) + [u_x u_z \cos\varphi_x + u_x u_y \sin\varphi_x](1 - \cos(\Omega_L t)). \tag{22}$$

Theoretical results for the time dependence of $\langle \sigma_x \rangle$ and $\langle \sigma_y \rangle$ are presented in Figure 2, with initial conditions $\langle \sigma_x(\tau = 0) \rangle = 1$ and $\langle \sigma_y(\tau = 0) \rangle = 0$. The spin time evolution contains two separate time dependencies. The main dependency is at the frequency precession Ω_L and the complex micro-motion is determined by the $\cos(\varphi_x(t))$ and $\sin(\varphi_x(t))$ functions producing the dressing frequency harmonics in Equation (18). The $\langle \sigma_x(t) \rangle$ time evolution of Figure 2a reports a direct Ω_L oscillation. Micro-motion oscillations at the ω and 3ω frequencies are instead present in the Figure 2b data for the $\langle \sigma_y(t) \rangle$ evolution. The Ω_L oscillation is derived from its envelope fit, as in the dashed red line of Figure 2b. Note

the initial $\langle\sigma_y\rangle(t=0) = 0$ condition imposed on the micro-motion oscillations. The spin time evolution was monitored by pick-up coils in Refs. [49,51,52]. The dressed response to RF pulses was measured in Ref. [48].
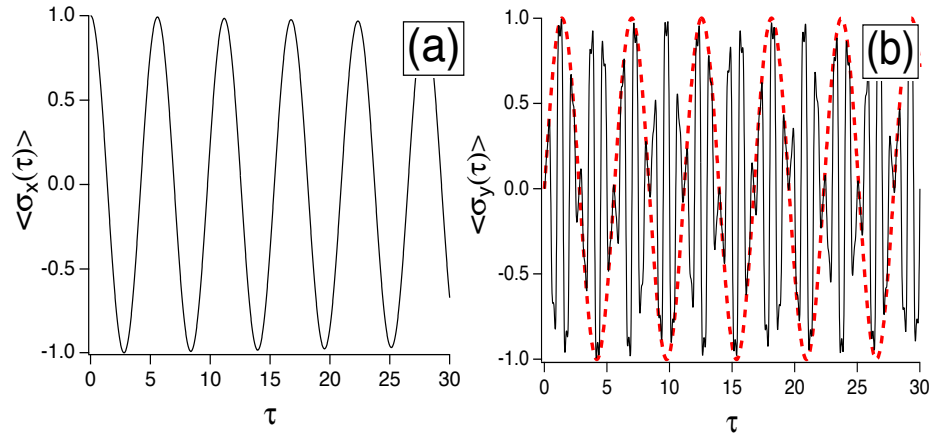
Figure 2. For the strong x single dressing, time evolutions of $\langle\sigma_x(\tau)\rangle$ (**a**) and $\langle\sigma_y(\tau)\rangle$ (**b**) versus the τ dimensionless time. Initial condition $\langle\sigma_x(\tau=0)\rangle = 1$. Here, $\Omega_x = 2\omega$, $\omega_{0z} = 0.8\omega$, and $\omega_{0x} = \omega_{0y} = 0$. The $\langle\sigma_x(\tau)\rangle$ oscillation takes place at Ω_L. The $\langle\sigma_x(\tau)\rangle$ evolution contains large micro-motion contributions at the ω and 2ω frequencies. In (**b**), the red dashed line represents the $\langle\sigma_y(\tau)\rangle$ time evolution envelope at the Ω_L frequency. See text for deatils.

3.3. Dual (x,y) Dressing

The bichromatic excitation of atoms/molecules is a powerful tool for spectroscopy based on the pump–probe operation of two applied electromagnetic fields. In this context, the pump action is quite often described by a dressed atom that we present below in Section 3.4. Here, we expand to two commensurate dressing fields [40,46,70], a strong dressing regime characterized by $\Omega_x \gg \omega$, as described in Section 3.2. We investigate the following Hamiltonian, written in the τ dimensionless time:

$$H(\tau) = \sum_{j=x,y,z} \frac{\omega_{0j}}{2\omega}\sigma_j + \frac{\Omega_x}{2\omega}\cos(\tau)\sigma_x + \frac{\Omega_y}{2\omega}\cos(p_y\tau + \Phi_{0y})\sigma_y. \tag{23}$$

The static field interaction is treated as a perturbation term. A perturbation treatment is also valid at low Ω_y/ω amplitudes. Within the strong dressing approach we apply to the time U and U_I evolution operators the gauge transformations of Equation (15). In addition we write for the U_I evolution operator a relation similar to Equation (16), with the present $A^{xy}(\tau)$ given by

$$A^{xy}(\tau) = e^{i\varphi_x(\tau)\sigma_x}\left[\frac{1}{2}\vec{\omega}_0 \cdot \vec{\sigma} + \frac{\Omega_y}{2\omega}\cos(p_y\tau + \Phi_y)\sigma_y\right]e^{-i\varphi_x(\tau)\sigma_x} = \frac{\omega_{0x}}{\omega}\sigma_x + g_y(\tau)\sigma_y + g_z(\tau)\sigma_z, \tag{24}$$

where

$$
\begin{aligned}
g_y(\tau) &= \frac{\omega_{0y}}{2\omega}\cos(\varphi_x) + \frac{\omega_{0z}}{2\omega}\sin(\varphi_x) + \frac{\Omega_y}{2\omega}\cos(\varphi_x)\cos(p_y\tau + \Phi_{0y}), \\
g_z(\tau) &= -\frac{\omega_{0y}}{2\omega}\sin(\varphi_x) + \frac{\omega_{0z}}{2\omega}\cos(\varphi_x) - \frac{\Omega_y}{2\omega}\sin(\varphi_x)\cos(p_y\tau + \Phi_{0y}).
\end{aligned}
\tag{25}
$$

The $\vec{h}^1$ first-order effective magnetic field is as follows:

$$\vec{h}^1 = (p_y, \text{even})\begin{pmatrix} \omega_{0x} \\ J_0(\tilde{\Omega}_x)\omega_{0y} + J_{p_y}(\tilde{\Omega}_x)\cos(\Phi_{0y})\Omega_y \\ J_0(\tilde{\Omega}_x)\omega_{0z} \end{pmatrix}; \quad (p_y, \text{odd})\begin{pmatrix} \omega_{0x} \\ J_0(\tilde{\Omega}_x)\omega_{0y} - J_{p_y}(\tilde{\Omega}_x)\sin(\Phi_{0y})\Omega_y \\ J_0(\tilde{\Omega}_x)\omega_{0z} \end{pmatrix}. \tag{26}$$

The Ω_L^1 dressed Larmor frequency is given by the $\vec{h}^1$ modulus. High-order corrections and numerical analyses are presented in Ref. [70]. The dual dressing produces a triaxial modification of the effective field, depending on the spatial direction of the applied magnetic field, i.e., an undressed response along the dressing field x direction and different scalings in the orthogonal axes.

The spectra of the λ_- and λ_+ Floquet eigenenergies and of the Ω_L frequency versus the dual dressing control parameters contain collapse/crossings and anticrossings similar to those reported in the x single dressing. In the present configuration, several control parameters exist, i.e., the Ω_x and Ω_y dressing frequencies, and the Φ_{0y} phase difference between the two dressing fields. Large p_y values lead to a smaller J_{p_y} contribution of the second dressing amplitude. For p_y, for even values, the second dressing field operate on the y component of the effective field (26), and on the z component for odd values. For $p = 2$ and $\omega_{0x} = 0$, a crossing of the eigenvalue is produced by appropriate combinations of the three control parameters, as shown in Figure 3a for Ω_L versus Φ_{0y}. For p_y odd values, three control parameters contribute to the h_z^1 component of Equation (26), opening up different crossing configurations, as presented in Figure 3b for Ω_L versus the Ω_x control parameter. The $p_y = 3$ plot of Ω_L versus Φ_{0y} is similar to the $p_y = 2$ one, except for the different Ω_L scale. For $\omega_{0x}, \omega_{0y} \neq 0$, all the crossings are transformed into anticrossings, as shown by the red dashed lines. The $\Omega_L > \omega_0$ correspond to $g_{\text{eff}} > 1$.
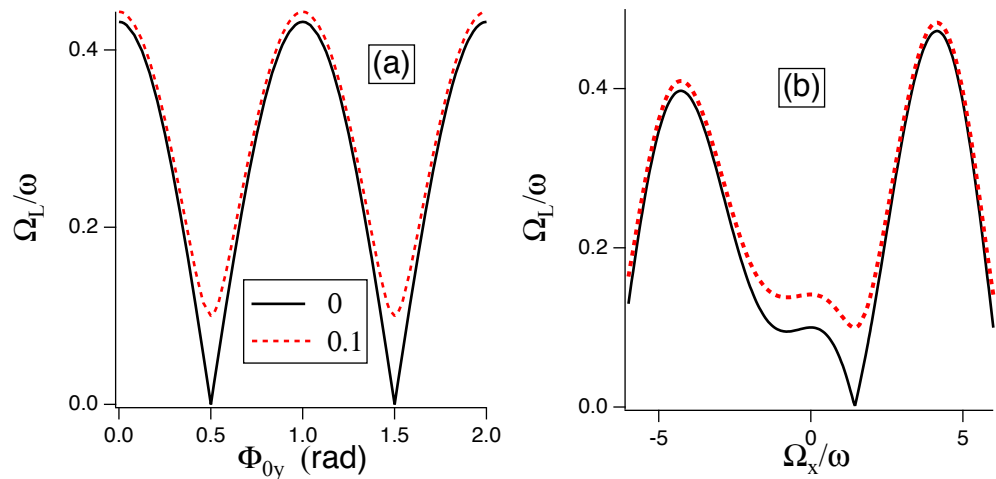
Figure 3. Spin response for (x, y) dual dressing. (**a**) $p_y = 2$: Ω_L versus Φ_{0y} for $\omega_{0x} = 0$ (black line) and $\omega_{0x} = 0.1\omega$ (red dashed line), as indicated; here, $\Omega_x = 2.405\omega$, $\omega_{0z} = 0.335\omega$, $\omega_{0y} = 0$. (**b**) $p_y = 3$: Ω_L versus Ω_x/ω for $\omega_{0x} = 0$ (black line) and $\omega_{0x} = 0.1\omega$ (red dashed line); here, $\omega_{0z} = 0.1\omega$, $\omega_{0y} = 0$, $\Omega_y = 2\omega$, and $\Phi_{0y} = \pi$. At the anticrossings, Ω_L is equal to ω_{0x}. Note the Ω_L maxima that is larger than the ω_{0z} value. See text for details.

3.4. Rotating Dressing

The rotating dressing case corresponds to the nuclear magnetic resonance configuration and has a simple solution. Its dressed atom analysis was presented in Ref. [71]. For a rotating RF/MW field with the Rabi frequency, Ω_R, the time evolution operator is given by

$$i\dot{U}(t) = \frac{1}{2}\omega_{0z}\sigma_z + \frac{1}{2}\Omega_R\left[\cos(\omega t)\,\sigma_x + \cos\left(\omega t + \frac{\pi}{2}\right)\sigma_y\right]U(\tau). \tag{27}$$

This evolution operator is equivalent to the U-operator (15) for the (x, y) dressing with $\Phi_{0y} = \pi/2$ and $\Omega_x = \Omega_y = \Omega_R$. However, the analysis of Section 3.3, valid for a x dressing larger than the y one, cannot be applied here to the magnetic resonance configuration, because the Floquet engineering approach is quite complex. The standard

approach of the transformation to a frame rotating around the *z*-axis at frequency ω leads to a time-independent problem. Within this frame, the $\vec{h}_{\text{rot}}$ effective field is

$$\vec{h}_{\text{rot}} = \begin{pmatrix} \Omega_R \\ 0 \\ \omega_{0z} - \omega \end{pmatrix}. \tag{28}$$

The corresponding E_+ and E_- eigenvalues are given by

$$E_\pm = \pm\frac{1}{2}\sqrt{(\omega_{0z} - \omega)^2 + \Omega_R^2}, \tag{29}$$

with $\Omega_L = |E_+ - E_-|$ for the Larmor frequency. The eigenvalues are plotted in Figure 4a versus the ω-normalized ω_{0z} field for different Ω_R values. The plots evidence the presence of crossings and anticrossings in the eigenenergies spectra. The eigenenergies position is at the $\omega_{0z} = \omega$ resonance. The crossing of E_+ and E_- occurring for $\Omega_R = 0$, i.e., the bare atom, is transformed into an anticrossing for $\Omega_R \neq 0$. An example of the associated $\langle P \rangle$ is plotted in Figure 4b versus ω_{0z}/ω at a small Ω_R value, as derived from Equation (10) with $\Omega_L = |E_+ - E_-|$. The maximum value of $\langle P \rangle$ occurs at the resonance value.
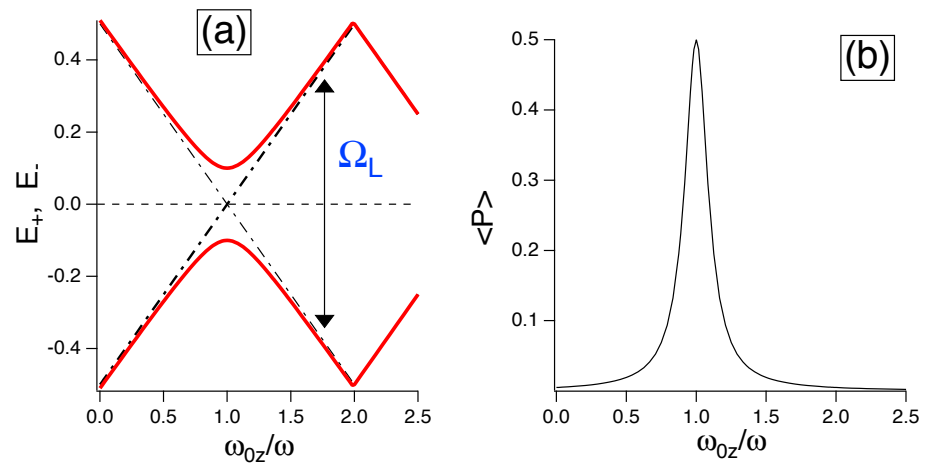
Figure 4. Rotating σ dressing at $\omega_{0x} = \omega_{0y} = 0$. (**a**) E_+ and E_- eigenenergies, normalized to the ω frequency, versus ω_{0z}/ω for $\Omega_R = 0$ (dashed-dotted black line) and $\Omega_R = 2\omega$ (solid red line). The Ω_L is given by the difference of the eigenenergies. (**b**) The time-averaged transition probability, $\langle P \rangle$, versus ω_{0z}/ω at $\Omega_R = 0.1\omega$.

3.5. Dual (x,z) Dressing

Here, the dressed atom approach is applied to the interaction of a spin with a static magnetic field and two RF fields—one *x*-polarized and the second one *z*-polarized. In the case of a large static magnetic field along the *z*-axis, the counter-rotating component of the *x*-field may be neglected. In this case, for the same driving frequency on the two axes and a static field on the *z*-axis only, we obtain the typical magnetic resonance configuration in the presence of a misalignment of the RF/MW field from orthogonality. This interaction has been examined in experiments on magnetic resonance and optical pumping. Theoretical analyses were presented in Refs. [28,42,72–74]. High-order perturbations and numerical solutions for the Λ stroboscopic matrix were also presented. Transition probabilities and RF shifts of the magnetic resonance produced by the misaligned RF field were verified in the experiments in Ref. [73,74].

Within the target of this study of the spin response at a low static field, we explore the influence of a misaligned RF field applied to a single, strong dressing configuration. We extend the magnetic resonance studies to the case of a misaligned RF field containing

harmonics of the main dressing. We investigate the following Hamiltonian written in dimensional units:

$$H(\tau) = \sum_{j=x,y,z} \frac{\omega_{0j}}{2\omega}\sigma_j + \frac{\Omega_x}{2\omega}\cos(\tau)\sigma_x + \frac{\Omega_z}{2\omega}\cos(p_z\tau + \Phi_{0z})\sigma_z. \tag{30}$$

Both the static field and Ω_z interactions are treated as perturbations to the strong x dressing field. Following the (x,y) treatment in Section 3.4, the U_I interaction evolution is determined by the following $A(\tau)$:

$$A(\tau) = e^{i\varphi_x(\tau)\sigma_x}\left[\frac{1}{2}\vec{\omega}_0 \cdot \vec{\sigma} + \frac{\Omega_z}{2\omega}\cos(p_z\tau + \Phi_{0y})\sigma_z\right]e^{-i\varphi_x(\tau)\sigma_x} = \frac{\omega_{0x}}{\omega}\sigma_x + f_y(\tau)\sigma_y + f_z(\tau)\sigma_z, \tag{31}$$

where

$$\begin{aligned} f_y(\tau) &= \frac{\omega_{0y}}{2\omega}\cos(\varphi_x) + \frac{\omega_{0z}}{2\omega}\sin(\varphi_x) + \frac{\Omega_z}{2\omega}\sin(\varphi_x)\cos(p_z\tau + \Phi_{0z}), \\ f_z(\tau) &= -\frac{\omega_{0y}}{2\omega}\sin(\varphi_x) + \frac{\omega_{0z}}{2\omega}\cos(\varphi_x) + \frac{\Omega_z}{2\omega}\cos(\varphi_x)\cos(p_z\tau + \Phi_{0z}). \end{aligned} \tag{32}$$

The $\vec{h}^1$ first-order effective magnetic field is

$$\vec{h}^1 = (p_z, even)\begin{pmatrix} \omega_{0x} \\ J_0(\tilde{\Omega}_x)\omega_{0y} \\ J_0(\tilde{\Omega}_x)\omega_{0z} + J_{p_z}(\tilde{\Omega}_x)\cos(\Phi_{0z})\Omega_z \end{pmatrix}; \quad (p_z, odd)\begin{pmatrix} \omega_{0x} \\ J_0(\tilde{\Omega}_x)\omega_{0y} - J_{p_z}(\tilde{\Omega}_x)\sin(\Phi_{0z})\Omega_z \\ J_0(\tilde{\Omega}_x)\omega_{0z} \end{pmatrix}. \tag{33}$$

A comparison between this effective field and the (x,y) dressing one of Equation (20) evidences quite a similar response, except for the different roles of the (even, odd) p_y and p_z parameters. For this configuration, the eigenvalues and dressed Larmor frequencies are equivalent to those in Figure 3 by choosing the proper control parameters.

4. Discussion and Conclusions

We presented a synthetic review of the interactions between atomic systems and the photons of an electromagnetic field. Those interatomic—or intermolecular—interactions play an important role in different phenomena and processes. An important branch of quantum control is based on the application or modification of an electromagnetic field made of either real or virtual photons, in order to drive the interactions toward a specific target. Such a quantum control area is broad enough, and different approaches have been devised to properly manipulate the available electromagnetic fields.

We only briefly examined the photon virtual dressing, which is the key element in quantum vacuum fluctuations and related phenomena such as the Casimir effect. Our analysis here concentrated on the quantum control by real photons. One issue is the resonant action of photons on the medium under investigation, where resonant exchanges occur between the bare atom and the dressing photons. This type of dressed control leads to changes in either population levels or energy splitting. The extension of resonant dressing to multilevel systems, another key aspect of quantum control, is not covered here. The second approach focuses on dressed states created by strong off-resonant electromagnetic fields, where the intensity surpasses the separation between the energy levels of interest. This method is mostly used today in laser-driven fusion. The strong dressing condition is also achieved when dealing with the Zeeman structure in quite low external magnetic fields. This regime of strong dressing by real photons interacting with a two-level structure forms the core of our analysis in this paper.

Although we have not treated virtual and real dressed treatments on equal footing, it is noteworthy to highlight the remarkable similarity between them. For instance, the formation of a dressed state with energy lower than the bare one occurs in a covalent crystal at zero temperature due to interaction with virtual longitudinal acoustic phonons,

and similarly in ultracold atoms due to interaction with real off-resonant photons. This is, actually, the basis of optical traps.

The main target of the real photon Floquet engineering is the quantum simulation. In the strong dressing configurations considered here, an effective static magnetic field with arbitrary direction and amplitude is produced. This result is not highly dramatic by itself, but interestingly enough, the amplitude of the effective field can be modified dynamically and precisely by controlling the amplitudes of the dressing fields. While the focus of this study was on the dressing by RF fields with commensurate frequencies, the application of incommensurate ones will open up new quantum simulation directions for Hamiltonians relevant to solid-state physics, as in Ref. [39]. The implementation of such configurations with RF incommensurate fields will represent an extension of the experiments quoted above for ground-state alkali atoms.

Concerning dressed atom experimental explorations, Rydberg atoms represent a new quantum control research area, as explored in Refs. [75–77]. For future investigations into dressed atoms, the recent efficient conversion of microwave photons to optical ones using strong microwave driving of Rydberg atoms, as seen in Ref. [78], opens a new field in hybrid quantum science. This offers prospects for producing "dressed" optical photons that acquire—in full—the atomic wave function features.

References

1. Compagno, G.; Passante, R.; Persico, F. *Atom-Field Interactions and Dressed Atoms*; Cambridge University Press: Cambridge, UK, 1995. [CrossRef]
2. Goldman, N.; Dalibard, J. Periodically driven quantum systems: Effective Hamiltonians and engineered gauge fields. *Phys. Rev. X* **2014**, *4*, 031027. [CrossRef]
3. Bukov, M.; D'Alessio, L.; Polkovnikov, A. Universal high-frequency behavior of periodically driven systems: From dynamical stabilization to Floquet engineering. *Adv. Phys.* **2015**, *64*, 139–226. [CrossRef]
4. Eckardt, A. Colloquium: Atomic quantum gases in periodically driven optical lattices. *Rev. Mod. Phys.* **2017**, *89*, 011004. [CrossRef]
5. Compagno, G.; Passante, R.; Persico, F. Edwin Power and the birth of dressed atoms. *Contemp. Phys.* **2006**, *47*, 269–278. [CrossRef]
6. Van Hove, L. The approach to equilibrium in quantum statistics: A perturbation treatment to general order. *Physica* **1957**, *23*, 441–480. [CrossRef]
7. Feynman, R.P. *QED: The Strange Theory of Light and Matter*; Princeton University Press: Princeton, NJ, USA, 1985. Available online: https://archive.org/details/qedstrangetheory00feyn (accessed on 5 December 2023).
8. Pekar, S.I.; Deigen, M.F. Quantum states and optical transitions of electron in a polaron and at a color center of a crystal. *Zh. Eksp. Teor. Fiz.* **1948**, *18*, 481–486. (In Russian). English translation: *Ukr. J. Phys.* **2008**, *53*, 78–82. Available online: http://archive.ujp.bitp.kiev.ua/files/journals/53/si/53SI17p.pdf (accessed on 5 December 2023).
9. Landau, L.D.; Pekar, S.I. Effective mass of a polaron. *Zh. Eksp. Teor. Fiz.* **1948**, *18*, 419–423. (In Russian). English translation: *Ukr. J. Phys.* **2008**, *53*, 71–74. Available online: http://archive.ujp.bitp.kiev.ua/files/journals/53/si/53SI15p.pdf (accessed on 5 December 2023).

10. Devreese, J.T.; Alexandrov, A.S. Fröhlich polaron and bipolaron: Recent developments. *Rep. Progr. Phys.* **2009**, *72*, 066501. [CrossRef]

11. Massignan, P.; Zaccanti, M.; Bruun, G.M. Polarons, dressed molecules and itinerant ferromagnetism in ultracold Fermi gases. *Rep. Progr. Phys.* **2014**, *77*, 034401. [CrossRef]

12. Compagno, G.; Passante, R.; Persico, F.; Salamone, G. Cloud of virtual photons surrounding a nonrelativistic electron. *Acta Phys. Pol. A* **1994**, *85*, 676–677. [CrossRef]

13. Compagno, G.; Passante, R.; Persico, F. The role of the cloud of virtual photons in the shift of the ground state energy of a hydrogen atom. *Phys. Lett. A* **1983**, *98*, 253–255. [CrossRef]

14. Passante, R.; Compagno, G.; Persico, F. Cloud of virtual photons in the ground state of the hydrogen atom. *Phys. Rev. A* **1985**, *31*, 2827–2841. [CrossRef] [PubMed]

15. Passante, R.; Power, E.A. Electromagnetic-energy-density distribution around a ground-state hydrogen atom and connection with van der Waals forces. *Phys. Rev. A* **1987**, *35*, 188–197. [CrossRef] [PubMed]

16. Passante, R. Dispersion interactions between neutral atoms and the quantum electrodynamical vacuum. *Symmetry* **2018**, *10*, 735. [CrossRef]

17. Cohen-Tannoudji, C.; Guéry-Odelin, D. *Advances in Atomic Physics: An Overview*; World Scientific: Singapore, 1994. [CrossRef]

18. Cohen-Tannoudji, C.; Haroche, S. Modification et annulation de facteur de Landé d'un atome couplage avec un champ de radiofréquence. *Comp. Rend. Acad. Sci. Paris B* **1966**, *262*, 268–271. Available online: https://gallica.bnf.fr/ark:/12148/bpt6k642 98075/f288.item (accessed on 5 December 2023).

19. Cohen-Tannoudji, C.; Haroche, S. Absorption et diffusion de photons optiques par un atome en interaction avec des photons de radiofréquence. *J. Phys. France* **1969**, *30*, 153–168. [CrossRef]

20. Landré, C.; Cohen-Tannoudji, C.; Dupont-Roc, J.; Haroche, S. Anisotropie des propriétés magnétiques d'un atome "habillé" par des photons de RF. *J. Phys. France* **1970**, *31*, 971–983. [CrossRef]

21. Ashhab, S.; Johansson, J.R.; Zagoskin, A.M.; Nori, F. Two-level systems driven by large-amplitude fields. *Phys. Rev. A* **2007**, *75*, 063414. [CrossRef]

22. Hausinger, J.; Grifoni, M. Dissipative two-level system under strong ac driving: A combination of Floquet and Van Vleck perturbation theory. *Phys. Rev. A* **2010**, *81*, 022117. [CrossRef]

23. Grifoni, M.; Hänggi, P. Driven quantum tunneling. *Phys. Rep.* **1998**, *304*, 229–354. [CrossRef]

24. Holthaus, M. Towards coherent control of a Bose-Einstein condensate in a double well. *Phys. Rev. A* **2001**, *64*, 011601. [CrossRef]

25. Bevilacqua, G.; Biancalana, V.; Dancheva, Y.; Moi, L. Larmor frequency dressing by a nonharmonic transverse magnetic field. *Phys. Rev. A* **2012**, *85*, 042510. [CrossRef]

26. Happer, W., Jr. Observations of transitions between stationary states in a rotating magnetic field. *Phys. Rev.* **1964**, *136*, A35–A42. [CrossRef]

27. Hofferberth, S.; Fischer, B.; Schumm, T.; Schmiedmayer, J.; Lesanovsky, I. Ultracold atoms in radio-frequency dressed potentials beyond the rotating-wave approximation. *Phys. Rev. A* **2007**, *76*, 013401. [CrossRef]

28. Allegrini, M.; Arimondo, E. Radiofrequency transitions in a dressed atom. *J. Phys. B At. Mol. Phys.* **1971**, *4*, 1008–1012. [CrossRef]

29. Harper, P.G.; Allegrini Arimondo, M. Resonant polaron damping of de Haas-Van Alphen oscillations in polar semiconductors. *J. Phys. C Solid State Phys.* **1971**, *4*, 181–186. [CrossRef]

30. Shirley, J.H. Solution of the Schrödinger equation with a hamiltonian periodic in time. *Phys. Rev.* **1965**, *138*, B979–B987. [CrossRef]

31. Sambe, H. Steady states and quasienergies of a quantum-mechanical system in an oscillating field. *Phys. Rev. A* **1973**, *7*, 2203–2213. [CrossRef]

32. Guccione-Gush, R.; Gush, H.P. Two-level system in a bichromatic field. *Phys. Rev. A* **1974**, *10*, 1474–1487. [CrossRef]

33. Chu, S.I.; Telnov, D.A. Beyond the Floquet theorem: Generalized Floquet formalisms and quasienergy methods for atomic and molecular multiphoton processes in intense laser fields. *Phys. Rep.* **2004**, *390*, 1–131. [CrossRef]

34. Blanes, S.; Casas, F.; Oteo, J.A.; Ros, J. The Magnus expansion and some of its applications. *Phys. Rep.* **2009**, *470*, 151–238. [CrossRef]

35. Leskes, M.; Madhu, P.K.; Vega, S. Floquet theory in solid-state nuclear magnetic resonance. *Prog. Nucl. Magn. Reson. Spectrosc.* **2010**, *57*, 345–380. [CrossRef] [PubMed]

36. Ivanov, K.L.; Mote, K.R.; Ernst, M.; Equbal, A.; Madhu, P.M. Floquet theory in magnetic resonance: Formalism and applications. *Prog. Nucl. Magn. Reson. Spectrosc.* **2021**, *126–127*, 17–58. [CrossRef] [PubMed]

37. Arnal, M.; Chatelain, G.; Cabrera-Gutiérrez, C.; Fortun, A.; Michon, E.; Billy, J.; Schlagheck, P.; Guéry-Odelin, D. Beyond effective Hamiltonians: Micromotion of Bose-Einstein condensates in periodically driven optical lattices. *Phys. Rev. A* **2020**, *101*, 013619. [CrossRef]

38. Desbuquois, R.; Messer, M.; Görg, F.; Sandholzer, K.; Jotzu, G.; Esslinger, T. Controlling the Floquet state population and observing micromotion in a periodically driven two-body quantum system. *Phys. Rev. A* **2017**, *96*, 053602. [CrossRef]

39. Martin, I.; Refael, G.; Halperin, B. Topological frequency conversion in strongly driven quantum systems. *Phys. Rev. X* **2017**, *7*, 041008. [CrossRef]

40. Fregosi, A.; Marinelli, C.; Gabbanini, C.; Bevilacqua, G.; Biancalana, V.; Arimondo, E.; Fioretti, A. Floquet space exploration for the dual-dressing of a qubit. *Sci. Rep.* **2023**, *13*, 15304. [CrossRef]

41. Pegg, D.T. Semi-classical model of magnetic resonance in intense RF fields. *J. Phys. B At. Mol. Phys.* **1973**, *6*, 246–253. [CrossRef]

42. Ruyten, W.M. Magnetic and optical resonance of two-level quantum systems in modulated fields. II. Floquet Hamiltonian approach. *Phys. Rev. A* **1990**, *42*, 4246–4254. [CrossRef]

43. Buckley, B.B.; Fuchs, G.D.; Bassett, L.C.; Awschalom, D.D. Spin-light coherence for single-spin measurement and control in diamond. *Science* **2010**, *330*, 1212–1215. [CrossRef]

44. Budker, D.; Kimball, D.F.; Rochester, S.M.; Yashchuk, V.V.; Zolotorev, M. Sensitive magnetometry based on nonlinear magneto-optical rotation. *Phys. Rev. A* **2000**, *62*, 043403. [CrossRef]

45. Fregosi, A.; Gabbanini, C.; Gozzini, S.; Lenci, L.; Marinelli, C.; Fioretti, A. Magnetic induction imaging with a cold-atom radio frequency magnetometer. *Appl. Phys. Lett.* **2020**, *117*, 144102. [CrossRef]

46. Bevilacqua, G.; Biancalana, V.; Vigilante, A.; Zanon-Willette, T.; Arimondo, E. Harmonic fine tuning and triaxial spatial anisotropy of dressed atomic spins. *Phys. Rev. Lett.* **2020**, *125*, 093203. [CrossRef]

47. Yabuzaki, T.; Tsukada, N.; Ogawa, T. Modification of atomic *g*-factor by the oscillating rf field. *J. Phys. Soc. Jpn.* **1972**, *32*, 1069–1077. [CrossRef]

48. Kunitomo, M.; Hashi, T. Modification of Zeeman energy by non-resonant oscillating field in the rotating frame. *Phys. Lett. A* **1972**, *40*, 75–76. [CrossRef]

49. Muskat, E.; Dubbers, D.; Schärpf, O. Dressed Neutrons. *Phys. Rev. Lett.* **1987**, *58*, 2047–2050. [CrossRef] [PubMed]

50. Gerbier, F.; Widera, A.; Fölling, S.; Mandel, O.; Bloch, I. Resonant control of spin dynamics in ultracold quantum gases by microwave dressing. *Phys. Rev. A* **2006**, *73*, 041602. [CrossRef]

51. Esler, A.; Peng, J.C.; Chandler, D.; Howell, D.; Lamoreaux, S.K.; Liu, C.Y.; Torgerson, J.R. Dressed spin of ^{3}He. *Phys. Rev. C* **2007**, *76*, 051302. [CrossRef]

52. Chu, P.H.; Esler, A.M.; Peng, J.C.; Beck, D.H.; Chandler, D.E.; Clayton, S.; Hu, B.Z.; Ngan, S.Y.; Sham, C.H.; So, L.H.; et al. Dressed spin of polarized ^{3}He in a cell. *Phys. Rev. C* **2011**, *84*, 022501. [CrossRef]

53. Beaufils, Q.; Zanon, T.; Chicireanu, R.; Laburthe-Tolra, B.; Maréchal, E.; Vernac, L.; Keller, J.C.; Gorceix, O. Radio-frequency-induced ground-state degeneracy in a Bose-Einstein condensate of chromium atoms. *Phys. Rev. A* **2008**, *78*, 051603(R). [CrossRef]

54. Pervishko, A.A.; Kibis, O.V.; Morina, S.; Shelykh, I.A. Control of spin dynamics in a two-dimensional electron gas by electromagnetic dressing. *Phys. Rev. B* **2015**, *92*, 205403. [CrossRef]

55. Hao, C.P.; Qiu, Z.R.; Sun, Q.; Zhu, Y.; Sheng, D. Interactions between nonresonant rf fields and atoms with strong spin-exchange collisions. *Phys. Rev. A* **2019**, *99*, 053417. [CrossRef]

56. Haroche, S. L'atome habillé: une étude théorique et expérirmentale des propriétés physiques d'atomes en interaction avec des photons de radiofréquence. Première partie. *Ann. Phys. Paris* **1971**, *14*, 189–326. [CrossRef]

57. Haroche, S. L'atome habillé: une étude théorique et expérirmentale des propriétés physiques d'atomes en interaction avec des photons de radiofréquence. Deuxième partie. *Ann. Phys. Paris* **1971**, *14*, 327–387. [CrossRef]

58. Bevilacqua, G.; Biancalana, V.; Dancheva, Y.; Vigilante, A. Sub-millimetric ultra-low-field MRI detected in situ by a dressed atomic magnetometer. *Appl. Phys. Lett.* **2019**, *115*, 174102. [CrossRef]

59. Haroche, S.; Cohen-Tannoudji, C. Resonant transfer of coherence in nonzero magnetic field between atomic levels of different *g* factors. *Phys. Rev. Lett.* **1970**, *24*, 974–978. [CrossRef]

60. Ito, H.; Ito, T.; Yabuzaki, T. Accumulative Transfer of transverse magnetic moment between spin-locked Rb and Cs atoms. *J. Phys. Soc. Jpn.* **1994**, *63*, 1337–1344. [CrossRef]

61. Golub, R.; Lamoreaux, S.K. Neutron electric-dipole moment, ultracold neutrons and polarized ^{3}He. *Phys. Rep.* **1994**, *237*, 1–62. [CrossRef]

62. Swank, C.M.; Webb, E.K.; Liu, X.; Filippone, B.W. Spin-dressed relaxation and frequency shifts from field imperfections. *Phys. Rev. A* **2018**, *98*, 053414. [CrossRef]

63. Pegg, D.T.; Series, G.W. Semi-classical theory of the Hanle effect with transverse static and oscillating magnetic fields. *J. Phys. B At. Mol. Phys.* **1970**, *3*, L33–L35. [CrossRef]

64. Cohen-Tannoudji, C.; Dupont-Roc, J.; Fabre, C. An experimental check of higher order terms in the radiative shift of a coherence resonance. *J. Phys. B At. Mol. Phys.* **1973**, *6*, L218–L221. [CrossRef]

65. Hannaford, P.; Pegg, D.T.; Series, G.W. Analytical expressions for the Bloch-Siegert shift. *J. Phys. B At. Mol. Phys.* **1973**, *6*, L222–L225. [CrossRef]

66. Ahmad, F.; Bullough, R.K. Theory of the Bloch-Siegert shift. *J. Phys. B At. Mol. Phys.* **1974**, *7*, L275. [CrossRef]

67. Series, G.W. A semi-classical approach to radiation problems. *Phys. Rep.* **1978**, *43*, 1–41. [CrossRef]

68. Stoneman, R.C.; Thomson, D.S.; Gallagher, T.F. Microwave multiphoton transitions between Rydberg states of potassium. *Phys. Rev. A* **1988**, *37*, 1527–1540. [CrossRef] [PubMed]

69. Zanon-Willette, T.; de Clercq, E.; Arimondo, E. Magic radio-frequency dressing of nuclear spins in high-accuracy optical clocks. *Phys. Rev. Lett.* **2012**, *109*, 223003. [CrossRef]

70. Bevilacqua, G.; Biancalana, V.; Zanon-Willette, T.; Arimondo, E. Harmonic dual dressing of spin-1/2 systems. *Phys. Rev. A* **2022**, *105*, 022619. [CrossRef]

71. Lo Cascio, L.; Persico, F. Strong-field theory of dressed atoms and dressed photons. *J. Mod. Optics* **1992**, *39*, 87–101. [CrossRef]

72. Pegg, D.T. Misalignment effects in magnetic resonance. *J. Phys. B At. Mol. Phys.* **1973**, *6*, 241–245. [CrossRef]

73. Yabuzaki, T.; Nakayama, S.; Murakami, Y.; Ogawa, T. Interaction between a spin-1/2 atom and a strong rf field. *Phys. Rev. A* **1974**, *10*, 1955–1963. [CrossRef]

74. Yabuzaki, T.; Murakami, Y.; Ogawa, T. Power shifts of multiphoton transitions in a spin 1/2 system. *J. Phys. B At. Mol. Phys.* **1976**, *9*, 9–19. [CrossRef]

75. Ni, Y.; Xu, P.; Martin, J.D.D. Reduction of the dc-electric-field sensitivity of circular Rydberg states using nonresonant dressing fields. *Phys. Rev. A* **2015**, *92*, 063418. [CrossRef]

76. Booth, D.W.; Isaacs, J.; Saffman, M. Reducing the sensitivity of Rydberg atoms to dc electric fields using two-frequency ac field dressing. *Phys. Rev. A* **2018**, *97*, 012515. [CrossRef]

77. Tommey, J.D.R.; Hogan, S.D. Resonant Rydberg-atom–microwave-field interactions in the ultrastrong-driving regime: Beyond the rotating-wave approximation. *Phys. Rev. A* **2019**, *100*, 053417. [CrossRef]

78. Kumar, A.; Suleymanzade, A.; Stone, M.; Taneja, L.; Anferov, A.; Schuster, D.; Simon, J. Quantum-enabled millimetre wave to optical transduction using neutral atoms. *Nature* **2023**, *615*, 614–619. [CrossRef]